Bright x-rays reveal shifting deformation states and effects of the microstructure on the plastic deformation of crystalline materials

A. J. Beaudoin
Cornell High Energy Synchrotron Source, Cornell University, Ithaca, New York 14853, USA
and Department of Mechanical Science and Engineering, University of Illinois at Urbana-Champaign, Urbana, IL 61801, USA

P. A. Shade, J. C. Schuren,* T. J. Turner, and C. Woodward
Materials and Manufacturing Directorate, Air Force Research Laboratory, Wright-Patterson Air Force Base, Ohio 45433, USA

J. V. Bernier and S. F. Li
Engineering Directorate, Lawrence Livermore National Laboratory, Livermore, California 94550, USA

D. M. Dimiduk
BlueQuartz Software, Springboro, Ohio 45066, USA
and Materials Science and Engineering, Ohio State University, Columbus, Ohio 43210, USA

P. Kenesei and J.-S. Park
Advanced Photon Source, Argonne National Laboratory, Argonne, Illinois 60439, USA
(Received 31 August 2017; revised manuscript received 9 November 2017; published 30 November 2017)

The plastic deformation of crystalline materials is usually modeled as smoothly progressing in space and time, yet modern studies show intermittency in the deformation dynamics of single-crystals arising from avalanche behavior of dislocation ensembles under uniform applied loads. However, once the prism of the microstructure in polycrystalline materials disperses and redistributes the load on a grain-by-grain basis, additional length and time scales are involved. Thus, the question is open as to how deformation intermittency manifests for the nonuniform grain-scale internal driving forces interacting with the finer-scale dislocation ensemble behavior. In this work we track the evolution of elastic strain within individual grains of a creep-loaded titanium alloy, revealing widely varying internal strains that fluctuate over time. The findings provide direct evidence of how flow intermittency proceeds for an aggregate of ∼700 grains while showing the influences of multiscale ensemble interactions and opening new avenues for advancing plasticity modeling.

DOI: 10.1103/PhysRevB.96.174116

I. INTRODUCTION

Systems such as moving tectonic plates, sea ice dynamics [1], and deforming crystalline metals are all examples of near-critical systems that exhibit stochastic, rapid energy dissipation under loading. Among these, the analysis of metal plasticity is important to the design, manufacture, and safe operation of structures under load. Automobiles, heavy machinery, and aerospace vehicles provide a few examples. At present, such analysis is based on phenomenological models tied directly to experimental protocols to form a design system. The manner for linking experimental measurements and the (tensorial) descriptions of stress and deformation are integral to models for design [2]. Thus, advances in experimental methods offer new opportunity for advancing model formulations to increase resolution and accuracy of analyzed loading states.

New experimental techniques are providing insight into the rich mechanical response of crystalline materials, beyond what can be gained through traditional mechanical testing. Studies using acoustic emission [3,4] and deformation of microcrystals [5,6] offer the exciting possibility of addressing the dynamics of plasticity and provide a pathway forward to developing models that are more faithful to the underlying mechanisms, even the possibility of a theory. A common objective in these single-crystal studies lies in characterizing plastic intermittency to understand apparent scale invariance at criticality, typically described by power-law distributions of crystal slip in space and time. The effects of temperature [7] and strain rate [8] have also received consideration.

Yet it is polycrystalline materials that appear ubiquitously in earthly systems, be they geologic or engineered by man. So extending this analysis of dynamics to these materials is crucial. Limited studies of polycrystalline materials using acoustic emission experiments [7,9,10], as well as dislocation dynamics simulations [11], point to the effects of microstructural features such as grain boundaries, without directly observing the behavior of grains transitioning through critical states in their natural surroundings. Intermittency at the scale of subgrains in a polycrystalline Cu was observed through reciprocal-space mapping using high-energy x-ray diffraction [12]. Access to the complex evolution in local driving forces resulting from the interactions between anisotropic elastic and plastic properties of individual grains within a polycrystalline aggregate is needed [13,14].

With these insights, we are motivated to develop high-energy x-ray diffraction methods to peer beyond the surface to within the material volume and to characterize the dynamics of

*Present address: DataRobot, Boston, Massachusetts 02110, USA.

elastic strain on a grain-by-grain basis in deforming polycrystalline samples. We utilize the following synchrotron radiation techniques: three-dimensional x-ray diffraction (3DXRD) [15] and high-energy diffraction microscopy (HEDM). The far-field variant of HEDM (FF-HEDM) makes possible the mapping of the elastic strain tensor on a grain-by-grain basis throughout the volume of a sample. With full strain tensors in hand, the corresponding Cauchy stress tensors may be obtained via application of a constitutive relation, i.e., Hooke's law [16–18]. The use of high-energy x rays from brilliant third-generation synchrotron sources facilitates measurement of the elastic strain distribution internal to the sample, where the stress state drives damage evolution, with temporal resolution. Studies of kinetics are possible, suggesting the possibility for tracking and quantifying temporal bursts in plastic activity [19].

The present work characterizes the dynamics of plastic relaxation events occurring during creep loading of a polycrystalline titanium alloy, showing that grain-level strains shift, both positively and negatively, in a correlated fashion between grains as time evolves. The measurement of evolving intergranular strain tensors which yield stress tensors *in situ* provides a mesoscopic view of the transient response through measures such as the resolved shear stress on a slip system. Identifying plastic events within individual grains associated with decreases in effective strain and collecting these events over the ensemble of grains tracked during the creep experiment enable the characterization of intermittency: a truly mesoscale description composed of local tensorial quantities in a bulk aggregate.

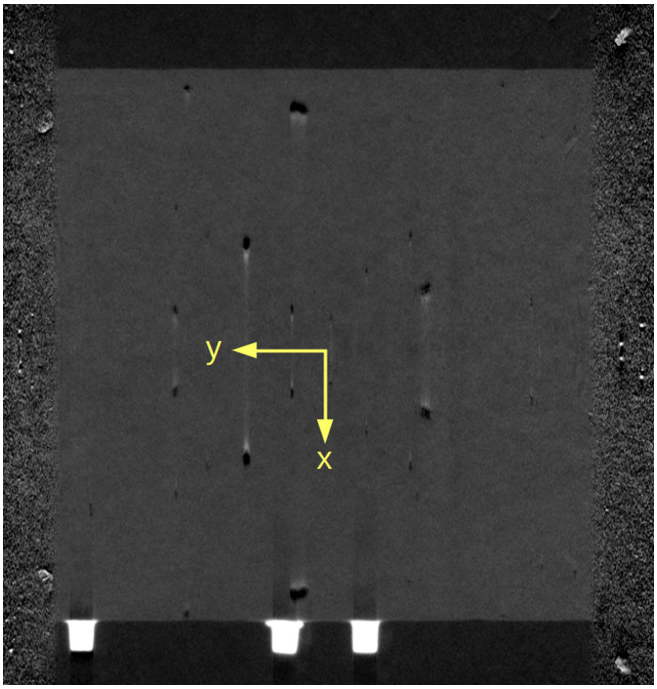

FIG. 1. CT reconstruction showing Au fiducial markers on the bottom $(+x)$ face. The markers, proceeding from left to right, are located at y positions of 0.435, 0.0675, and -0.0547 mm. These positions were established by averaging the position of indexed Au grains contained in the markers. The tensile direction is along the horizontal.

II. MATERIALS AND METHOD

A. In situ mapping of elastic strain

1. Creep loading of the Ti7 sample

The alloy Ti-7Al was utilized in this work and has a composition similar to the α phase in many commercially relevant titanium alloys. Material was cast, extruded, and heat treated to produce single-phase α (hcp crystal structure) with equiaxed grains and an average grain size of $\sim$75 μm [20]. The presence of Al suppresses twinning in this alloy [21]. The heat treatment procedure included air cooling from a temperature of 962 °C that promoted short-range ordering and the formation of nanoscale Ti_3Al precipitates [22]. Furthermore, due to anisotropic thermal expansion, the heat treatment procedure led to the presence of residual stresses at the individual grain scale, which is likely to influence the deformation behavior [23]. Its nominal yield stress σ_y is 610 MPa. The sample was cut out with an electrical discharge machine (EDM) and then lightly electropolished, which smoothed out any sharp surface roughness yet still preserved some of the surface topography from the EDM sufficient to perform digital image correlation (DIC). The sample had a nominal gauge volume of $1 \times 1 \times 8$ mm^3. Three fiducial markers of Au [24] were placed on the sample surface, with normal in the $+x$ direction (Fig. 1). These markers enabled the spatial correlation between DIC images, computed tomography (CT) reconstructions, and grain position from analysis of diffraction patterns. CT data were analyzed using the GRIDREC algorithm [25,26]. The DIC images were utilized to calculate macroscopic strains through a two-point tracking algorithm.

For study *in situ*, we utilized a rotational and axial motion system (RAMS) load frame insert device [27] that was inserted in an MTS servohydraulic model 858 load frame at the high-energy beamline 1-ID-E of the Advanced Photon Source (APS), Argonne National Laboratory (Fig. 2). This setup enabled the sample to be loaded axially in tension while independently rotated over 360° to collect HEDM and CT data *in situ*.

The x-ray energy was 65.351 keV. The diffraction data were collected with a box x-ray beam that was approximately 1.5 mm wide by 1.0 mm tall and a large panel area detector that was placed approximately 1 m from the sample.

The sample was loaded in uniaxial tension in steps, first to 23% of the yield stress σ_y, then to 47% and 70% of yield, to capture some baseline information about the sample in the elastic state. The sample was then held at $0.8\sigma_y$ for 17 h and $0.85\sigma_y$ for 24.4 h. During the creep loading, FF-HEDM and DIC images were collected in a continuous fashion; the time to perform a complete scan was approximately 14.5 min. CT data were also collected before and after the creep-loading experiment. The experimental data collected at $0.85\sigma_y$ demonstrated significant plastic activity and will serve as the focus for the current study.

2. Analysis of diffraction patterns

Diffraction images were processed using the HEXRD analysis software [18,28]. This software identifies and indexes

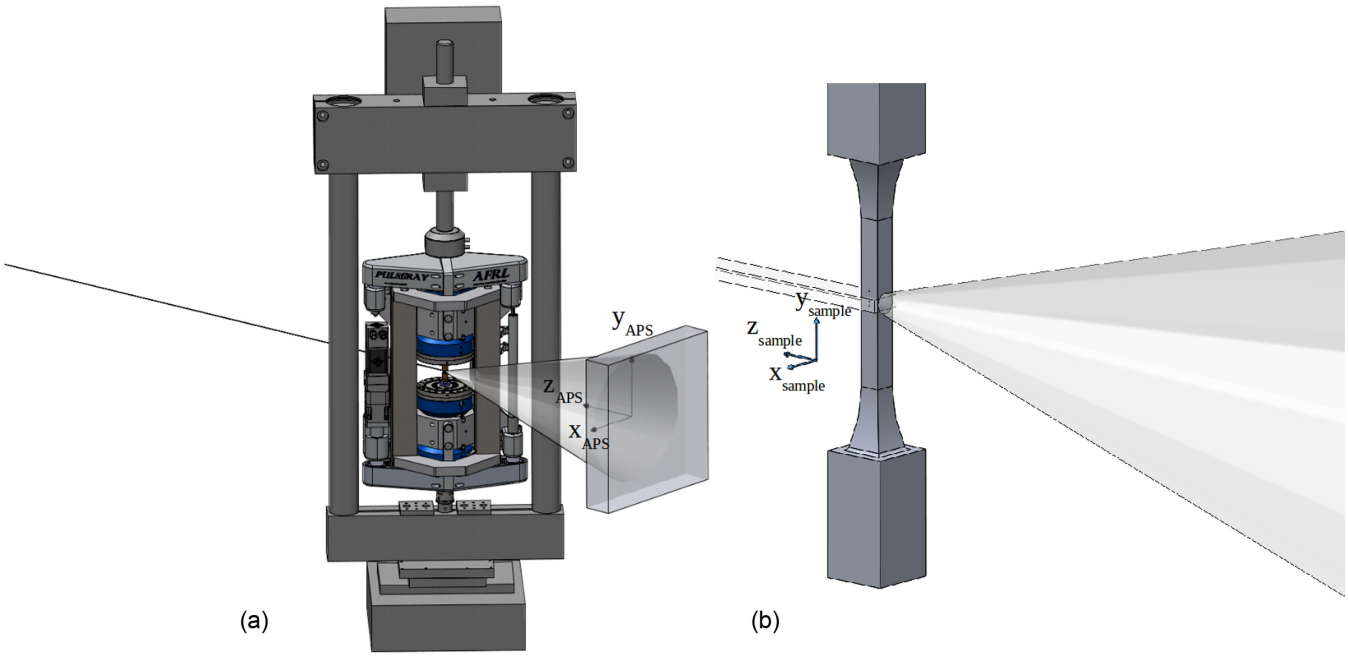

FIG. 2. Experimental configuration showing laboratory (APS) and sample coordinate systems.

individual grains in the illuminated cross section, providing lattice orientation, grain center-of-mass position, and the elastic strain $\boldsymbol{\varepsilon}$ (note that all quantities given in the paper refer to the average over a grain, unless stated otherwise). Stress $\boldsymbol{\sigma}$ was derived from the elastic strain tensor and single-crystal elastic constants [22].

The "goodness of fit" χ^2 is calculated for each grain by summing the squared residuals between the measured and predicted elastic stretch, orientation, and position and then normalizing by degrees of freedom. The requirement $\chi^2 < 0.002$ was taken for grains contributing to analysis of intermittency below. Using this metric, ~700 indexed grains were included in the subsequent analysis. Completeness, the ratio of detected to expected diffraction signals for an indexed grain, had minimum and average values of 57.9% and 99.98%, respectively [29].

There are several possible contributions to error in the volumetric strain of the lattice and, in turn, the hydrostatic stress. Therefore, a correction to the stress was made through the use of the Au fiducial markers. Since the markers lie on the surface of the sample and are unloaded, any variations in mean strain within the markers must correspond to variations in experimental conditions. The volumetric strain of the Au was first correlated with that of the Ti-7Al average, and corrections were then made to the stress for each grain through a correction to the mean (hydrostatic) stress, defined as $\sigma_m = \mathrm{tr}(\boldsymbol{\sigma})/3$. Note that this correction is small, within ± 0.0001 for the volumetric strain $\Delta V/V$.

The effective stress σ_{eff} is computed as

$$\sigma_{\mathrm{eff}} = \sqrt{\tfrac{3}{2}\boldsymbol{\sigma}' : \boldsymbol{\sigma}'}, \tag{1}$$

where the stress deviator is $\boldsymbol{\sigma}' = \boldsymbol{\sigma} - \sigma_{\mathrm{m}}\mathbf{I}$, where $\mathbf{I}$ is the identity tensor. Similarly, the effective strain follows from

$$\varepsilon_{\mathrm{eff}} = \sqrt{\tfrac{2}{3}\boldsymbol{\varepsilon}' : \boldsymbol{\varepsilon}'}, \tag{2}$$

where $\boldsymbol{\varepsilon}' = \boldsymbol{\varepsilon} - \varepsilon_{\mathrm{m}}\mathbf{I}$ and $\varepsilon_{\mathrm{m}} = \mathrm{tr}(\boldsymbol{\varepsilon})/3$.

Time series data for the stress and strain for each grain were processed using a simple first-order difference to give rate of change.

B. Analysis of intermittency

Intermittent plastic flow is often characterized through a power-law relationship [3,6,7,9,11,30–32],

$$P(x) \propto x^{-\alpha}, \tag{3}$$

where $P(x)$ is the probability distribution for dissipation events of size x and α is the scaling exponent. The exponent is developed through the maximum likelihood estimator (MLE) following Clauset *et al.* [33], computed as

$$\alpha = 1 + n\left[\sum_{i=1}^{n} \ln \frac{x_i}{x_{\min}}\right]^{-1}. \tag{4}$$

The MLE was evaluated using the power-law package [34], combining the data for the two loading cases of $0.8\sigma_y$ and $0.85\sigma_y$. Using the grain-scale resolution attained for this study, the dissipation sizes occurring for individual grains make up the analyzed populations, even though multiple dissipation events may have occurred during the same scan (time) window. Analysis of the collective dissipation event populations awaits further study.

Events x_i are based on the decrease in effective elastic strain, $\Delta\varepsilon_{\mathrm{eff}} < 0$, in units of microstrain. The reason for this particular choice is to draw some basis of comparison between studies of microcrystals [5,6,8,30] and the present study. Implicit in the analysis of plastic events in the loading of micropillars is the assumption that the change in elastic strain is small: the deformation increment essentially corresponds to a plastic strain increment. In the creep deformation considered herein, a stress relaxation event is associated with a decrease in

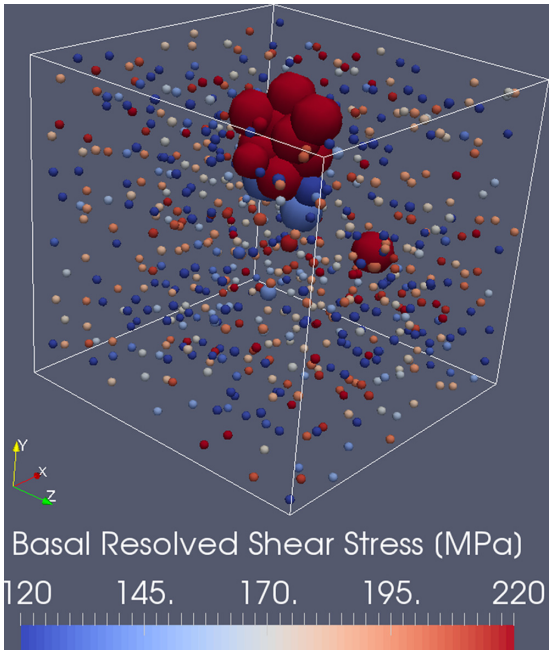

FIG. 3. Grains in the 1 mm^3 region illuminated by high-energy x rays. Grains tracked during creep at $0.85\sigma_y$ are shown as spherical symbols. The symbol color corresponds to the maximum resolved shear stress for basal slip, and the size corresponds to the relaxation (decrease) of the effective stress over the duration of the scan (∼15 min). The origin is located at the center of the cube outline. The scan was taken at 3.3 h into the creep loading.

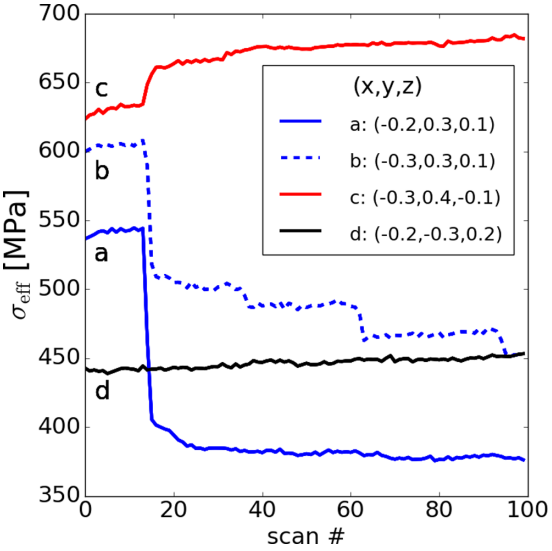

FIG. 4. Grains at $y = 0.3$ in a cluster (relaxing grains of Fig. 3) that shows a large transient (grain a), several transients of varying magnitude (grain b), and loading of a grain (grain c) adjacent to the cluster containing grains a and b. By comparison, grain d, located at approximately the same cross-sectional region but at a different vertical location along the tensile axis, $y = -0.3$, exhibits relatively quiescent behavior. The inset relates the position of the grains with respect to the center of the cube outline of Fig. 3.

the elastic strain and a concomitant (deviatoric) plastic strain increment. Considering that the total deformation between measurements is small during the creep loading, this grain-scale plastic strain increment may be (roughly) associated with a decrease in the effective elastic strain. When comparing scaling exponents from the present work with values in the literature relating to dissipative measures, there is the implicit assumption that the incremental (creep) strain in a grain is small with respect to the decrease in elastic strain; this will have the effect of truncating large events, for which this assumption does not hold.

Decreasing transients in the ε_{eff} signal were identified as sequential scans with negative backward difference values, and events were characterized as the magnitude of the decrease through the transient. At least two sequential scans with a negative rate were required for identification as a transient event, and we note that this condition slightly biases the data by omitting the smallest events.

III. RESULTS

A. Collective response of grains

We turn first to the response extending beyond single grains: plastic events occurring across aggregates of grains and extending to bending forces that span the sample cross section. Figure 3 shows a frame from the video in the Supplemental Material [35]. The technique employed in the present work enables not only the determination of grain location within the sample but also resolved shear stress on active slip systems: the symbol locations correspond to grain centroids; the symbol color corresponds to the maximum resolved shear stress for basal slip systems in units of megapascals for the corresponding grain, and the size of the symbol is scaled to the magnitude of decrease in the effective stress between scans. There is collective relaxation of a cluster of grains. Most of these grains show a large driving force for basal slip. Note that the applied macroscopic tensile stress remains constant in spite of the observed mesoscale fluctuations. A three-dimensional visualization of the complete time series is available in the Supplemental Material.

Several other plastic relaxation events involving multiple grains are evident in the video presented in the Supplemental Material. Such a localized response (although extensive in the sense of following from a grain aggregate), combined with spatial gradients in grain crystallographic orientation, form a microstructural prism that modifies the long-range stress state. As a specific example, the collective action of localized plastic events is evident through the release of a bending moment, associated with sample-scale gradients in driving force for prismatic slip (Appendix). In a call and response fashion, dislocation avalanches occurring in individual grains must respond to this change in long-range stress.

B. Response of individual grains

A key advantage of the present technique is the capability to identify avalanchelike behavior developed within individual grains. Several grains in the region of the large symbols in Fig. 3 provide insight into the localized stress transient. Numerous grains show a large decrease in the effective stress; examples are evident in grains a and b in Fig. 4. Note that the

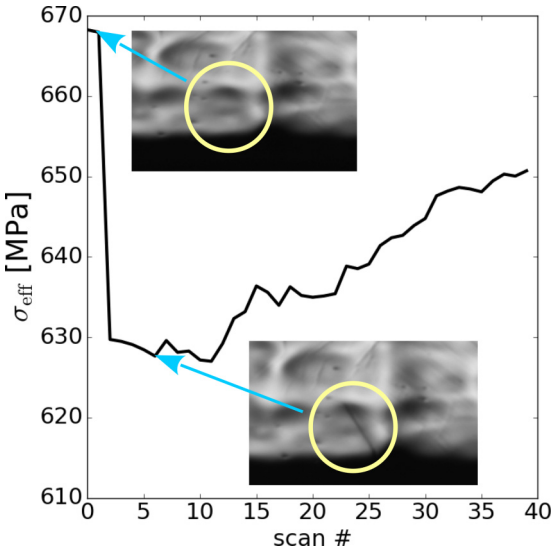

FIG. 5. Stress decrease at the outset of creep loading at 85% of the yield stress, with corresponding slip band developed at the location of the grain (illustrated using DIC images).

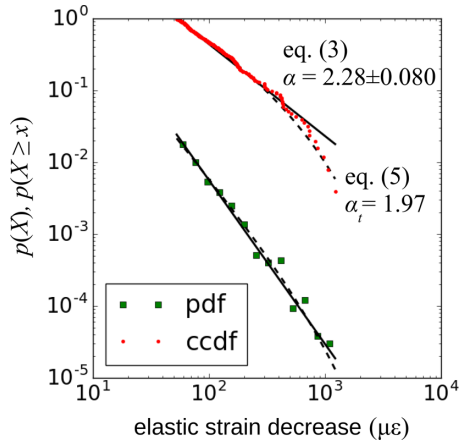

FIG. 6. Scaling developed through unloading events for effective elastic strain (horizontal axis, in units of $\mu\varepsilon$), combining events from the $0.8\sigma_y$ and $0.85\sigma_y$ loading cases. Solid and dashed lines show fits to Eqs. (3) and (5), respectively. The event populations consist of relaxation events occurring within individual grains, even though some of the events occurred in the same time window.

effective stress decrease occurring around scan 12 generally progresses over three or more (complete) scans. The error is small, with maximum residual for fitting of diffraction vectors χ^2 of roughly 0.001 for grain b and other grains showing smaller errors. This is to suggest confidence in the evaluation of elastic strain transients. Note that these stress relaxation events may be quite large, on the order of 150 MPa (∼30% of the applied load). The temporal history for a grain situated adjacent to the relaxing cluster of Fig. 3 is provided by grain c in Fig. 4; this highlights the load transfer occurring during the relaxation of the grain aggregate.

For comparison, a grain in the same cross-sectional vicinity of the relaxing aggregate shown in Fig. 3 but located at a different y location along the specimen tensile axis exhibits many small relaxation events about a slightly increasing effective stress (grain d in Fig. 4). Note that the maximum resolved stress for prism slip is quite small for the grain shown, with a maximum value of 19.8 MPa, well below the prismatic slip system strength of 220–260 MPa for this material [36]. Considering the possibility of basal slip, the maximum resolved shear stress developed over the course of creep is just 60.4 MPa, again, well below the expected strength.

The DIC images showed many instances of intermittent plastic activity through the presence of slip bands. One example is a slip band developing in the corner of the sample early in the course of creep at $0.85\sigma_y$ (Fig. 5). Using the position of the fiducial markers on the corresponding DIC images and HEDM indexing, the grain at this location was identified. The stress history shows a distinct stress relaxation event, on the order of 40 MPa, upon initial loading.

C. Observation of intermittent plasticity

Plots of the probability density function $p(X)$ and complementary cumulative distribution function $p(X \geqslant x)$ for decreases of the effective strain are shown in Fig. 6. The value of $x_{\min}$ is $52\mu\varepsilon$. The fit to Eq. (3), using the MLE, is given as a solid line.

A power law with cutoff,

$$P_t(x) \propto x^{-\alpha_t} e^{-\lambda x}, \tag{5}$$

is also shown as a dashed line in the plots of Figure 6. Here, α_t is the exponent associated with the presence of a multiplicative exponential cutoff. For the dashed lines in Fig. 6, λ was found to be 0.001. Consideration of the likelihood ratio test [37,38], as discussed by Clauset *et al.* [33], indicates a power law with cutoff, with $p = 0.015$; the case of an exponential distribution may be ruled out with $p = 0.001$. The number of events contributing to the exponent is 255. Taking only the case of the $0.85\sigma_y$ creep loading renders essentially the same exponents, $\alpha = 2.25 \pm 0.088$ and $\alpha_t = 1.97$, with a total of 199 events.

A key advantage to the present technique is the capability to identify the driving forces for slip on a grain-by-grain basis. Events contributing to the evaluation of the MLE are plotted in Fig. 7. The magnitudes of the relaxation events $\Delta\varepsilon_{\text{eff}}$ are plotted against the maximum value of resolved shear stress at the beginning of the relaxation event for prism slip and basal slip. The maximum resolved shear stress is taken as the maximum over possible slip systems for a particular slip mode, basal or prism. The symbols are colored according to the basal slip system's maximum resolved shear stress. There is a trend in which the largest relaxation events are associated with basal slip.

IV. DISCUSSION

The coordinated application of high-energy x-ray diffraction, x-ray tomography, and DIC was carried out to study spatiotemporal strain evolution in a polycrystalline Ti-7Al sample held near the critical state (creep loading). Through the use of single-crystal elastic constants, the stress tensor was recovered on a grain-by-grain basis at regular intervals during the *in situ* deformation. Several different measures related to

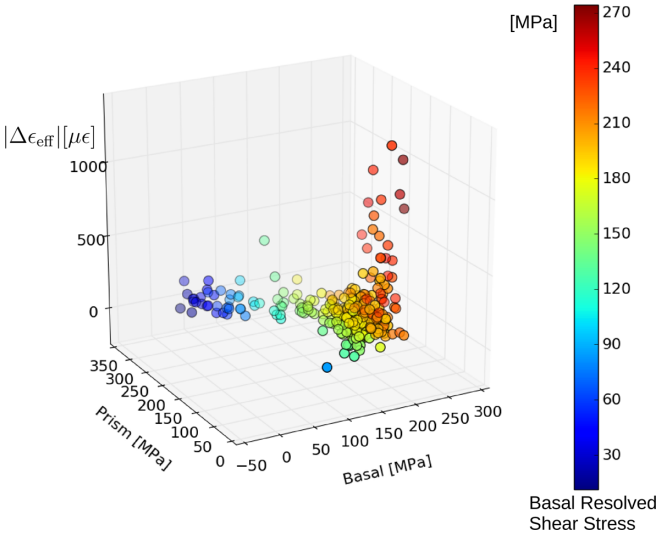

FIG. 7. Relaxation events as measured by change (magnitude of decrease) in effective strain, plotted against maximum resolved basal and prism slips.

the deformation state were evaluated from the stress tensor history. Transient stress relaxation events were identified at the scale of individual grains, as well as for collections of grains. Relaxation transients were directly coupled to the development of slip bands through comparison of stress history and optical DIC images.

Our high-energy synchrotron x-ray-based characterization method allows us to measure the temporally resolved full elastic strain tensor of each one of these 700 crystals throughout the experiment. The experiment provides direct information about which grains are deforming, their spatial locations within the specimen, their micromechanical state, and their relationships to local grain neighborhoods. This allows direct observation of the spatial correlation of deformation events in individual grains. Furthermore, the tensorial nature of our measurement allows us to consider different metrics for quantifying the intermittent behavior such as the stress resolved on a slip system, effective stress, and effective strain.

Plasticity bursts occur during the creep loading of Ti-7Al. There is a clear spatiotemporal aggregation of discrete events that takes place. Some transients resulted from the collective dissipative action of several grains, providing clear indication that the maximum avalanche size extends beyond the size of the strain attained in a single grain [7]. Also, resolving the correlated grain neighborhoods shows that dissipation occurring at criticality for a given grain leads to elastic unloading of that grain and load shedding to neighboring grains. Thus, a unique attribute of the polycrystalline condition, relative to common testing of single crystals, is that both the driving forces and the dissipation mechanisms involve correlated ensembles acting at multiple scales.

In general, the power-law scaling exponent has a magnitude similar to that observed in studies of LiF microcrystals [30]. The data bring into view the fact that slip system geometry provides a spectrum of loading and dissipation conditions in a bulk polycrystalline aggregate. Collective relaxation of a grain cluster was observed, as was the development of a slip band in a single surface grain as its internal stress relaxed. These dissipative events, together with changes in the driving force during dissipation, may contribute to the observed exponent, depending upon the data collection and analysis methods. The exponents found in the present work are greater than the $\alpha \approx 1.4$ suggested by mean-field theories [39] and $\alpha \approx 1.35$ observed for ice polycrystals [7]. There are several considerations to be made in assessing such differences.

(i) The intermittency in the present study likely includes different mechanisms: the effect of the solute and/or ordering of the solute, rate dependence of different slip modes, and collective dislocation motion. In addition, there appear to be grains that undergo little plasticity, exhibiting a transient response that reflects the long-range stresses (and not plastic relaxation local to the grain).

(ii) Relative to other techniques, the time resolution of the experiments is low, and the scaling results are missing the smallest part of the strain-burst population. Also, it is not clear how the effective strain considered herein would relate to acoustic emission or microcrystal studies. Further theoretical development is needed on this point.

(iii) Similar to the role of test apparatus stiffness in the measurements of single crystals [40,41], elastoplastic relaxations about a given grain in a polycrystalline material locally reduce the driving force for the flow of that grain.

Further interpretation may be drawn from the literature. Given these considerations and knowledge of the low time resolution for the study, one cannot rule out that there exists a balance of intermittent and continuous plastic flow in this bulk sample [10], and short-range dislocation interactions may contribute to a Gaussian-like background flow. In any case, the collective relaxation of several grains is consistent with acoustic emission data showing spatial correlation of dislocation avalanches in polycrystalline ice [7].

As another alternative, a scaling exponent of ~ 2 for a power law is consistent when taking events over a range of applied stress [32,42,43]. Such an integrated exponent is relevant to the present study. While the loading is constant in the sample reference frame, the resolved shear stress driving slip varies locally due to slip system geometry (orientation) and anisotropic elasticity. Thus, the overarching microstructure alters the stresses in the lattice reference frame, such that each grain sees different driving forces for dissipation.

Notions set forth by Brown [44,45] present an explanation relevant to the slip character and microstructure of the Ti-7Al alloy studied herein. He proposes that an exponent of ~ 1.5 may be expected when the spread of a slip band is limited by secondary slip or twinning. Should the spread be limited by features independent of the applied stress, the expected scaling is $\alpha \approx 2$. The presence of short-range ordering [22,46] contributes to a planar slip character [47,48], lessening the coactivation of other slip modes within a grain. That intermittency is associated with activation of a single slip mode within a grain is consistent with the dominance of basal slip [44] as a contributor to large relaxation events (Fig. 7). The area spanned by a slip band is, in turn, limited through intrinsic features of the microstructure, such as change in crystallographic orientation, and hence the driving force for slip, at grain boundaries or outside a cluster of similarly oriented grains.

V. SUMMARY

We have described direct observation of deformation intermittency at the individual grain level of a polycrystalline ensemble using a tensorial description of elastic strain and stress through application of *in situ* HEDM experiments. While the time needed to collect diffraction patterns implies averaging over many smaller events, it is possible with present technology to identify the collective response of several grains, over several scans of the sample. Advances in detector technology are rapid, and we foresee an order-of-magnitude improvement in the time to collect images. The next step is the consideration of intermittency in the context of the constitutive laws that form the basis of physically based models for plasticity. In such a pursuit, words of caution with regard to different alloy systems are warranted (see the end of Sec. 4 of Sethna *et al.* [49]). For the material in the present study, many large events occurred early in the creep loading, consistent with the deviation from a steady-state creep response at short times [46], as associated with local rearrangement of internal stress in this alloy system [50]: each grain sees different, sometimes rather rapid, decay of the driving force once an unloading event starts. Thus, the dissipation might be artificially truncated relative to the more constant driving force for microcrystals. Still, there exists some common character to the organization of relaxation events to form avalanches with different deformation mechanisms [51]. Works that provide consideration of distinct mechanisms in the context of avalanche formation offer a path for further study [45]. While there remains much to consider in interpretation of the present results, the technique presented herein offers a pathway to extending the research of intermittency to bulk samples with sufficient resolution to advance constitutive models for metal plasticity.

A new approach to deformation and damage models incorporating spatiotemporal intermittency that is informed and validated through experiments such as that described in the present paper may invigorate ongoing efforts to develop and integrate computational tools for structural materials engineering. For example, it is well known that fatigue cracks tend to initiate where plastic strain has been concentrated into a localized region (e.g., slip bands) [52], yet the corresponding intermittent deformation behavior cannot be predicted by modern crystal plasticity codes. Developing a deeper understanding of this phenomenon may offer exciting opportunities for engineering a desired response from the material [53].

ACKNOWLEDGMENTS

Discussions with Prof. K. Dahmen and Prof. R. Maass of the University of Illinois at Urbana-Champaign provided insight into interpretation of the results. The Ti-7Al material was provided by A. Pilchak of the U.S. Air Force Research Laboratory. The authors are grateful to B. Blank, A. Mashayekhi, and J. Almer for experimental support. Constructive criticism by reviewers improved the manuscript, and we also thank an anonymous reviewer who pointed out the connection between the present research and interpretations set forth by L.M. Brown. Support from the Materials and Manufacturing Directorate of the U.S. Air Force Research Laboratory is acknowledged. A.J.B. received support through Air Force contract FA8650-14-D-5205/0001. Use of the Advanced Photon Source, an Office of Science User Facility operated for the U.S. Department of Energy by Argonne National Laboratory, was supported under Contract No. DE-AC02-06CH11357.

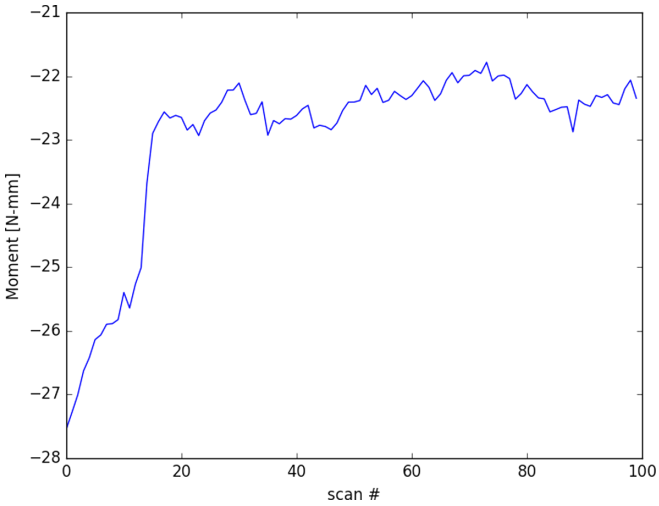

FIG. 8. Bending moment developed at $y = 0.35$ mm along the tensile axis.

APPENDIX: BENDING MOMENT

The collective stress release shown in Fig. 3 is associated with transient behavior of the bending moment. The moment is a consequence of gradients in crystallographic orientation across the sample and the subsequent grain-to-grain variation in ability to sustain load. The moment was developed by summing the stress component in the direction of loading σ_y as $M_{zy} = \sum_g \sigma^g_{yy} x^g A$ for grains within the slice $0.225 \leqslant y \leqslant 0.475$ (Fig. 8). This volume spans the grain aggregate exhibiting the stress decrease in Fig. 3. An estimate of the cross-sectional area for a grain, $A = 0.018\,\text{mm}^2$, was developed by computing the average volume V of a grain g contained within the slice and then calculating the area as $A = V^{\frac{2}{3}}$. The moment relaxed from -27.5 to -22.9 N mm from the beginning of creep at $0.85\sigma_y$ through the course of the event illustrated in Fig. 3.

The capability to track the response for individual grains further enables the means to establish a link between this bending moment and spatial gradients in crystallographic orientation by the difference in the maximum resolved shear stress on prism planes on the $-x$ and $+x$ sides of the sample over time. Averaging over grains within 0.1 mm of the sides of the sample gives a resolved shear stress of 130 and 180 MPa for the $-x$ and $+x$ sides of the sample, respectively. This higher driving force for prismatic slip on the $+x$ face is reinforced by the DIC results, which show an increased total strain of 0.0014 on the $+x$ side of the sample, relative to the $-x$ side.

[1] D. Marsan and J. Weiss, Earth Planet. Sci. Lett. **296**, 353 (2010).

[2] D. M. Dimiduk and S. Ghosh, *Computational Methods for Microstructure-Property Relationships* (Springer, Berlin, 2011).

[3] M. C. Miguel, A. Vespignani, S. Zapperi, J. Weiss, and J. R. Grasso, Nature (London) **410**, 667 (2001).

[4] J. Weiss and D. Marsan, Science **299**, 89 (2003).

[5] D. M. Dimiduk, C. Woodward, R. Lesar, and M. D. Uchic, Science **312**, 1188 (2006).

[6] M. D. Uchic, P. A. Shade, and D. M. Dimiduk, Annu. Rev. Mater. Res. **39**, 361 (2009).

[7] T. Richeton, J. Weiss, and F. Louchet, Acta Mater. **53**, 4463 (2005).

[8] S. Papanikolaou, D. M. Dimiduk, W. Choi, J. P. Sethna, M. D. Uchic, C. F. Woodward, and S. Zapperi, Nature (London) **490**, 517 (2012).

[9] T. Richeton, J. Weiss, and F. Louchet, Nat. Mater. **4**, 465 (2005).

[10] J. Weiss, W. B. Rhouma, T. Richeton, S. Dechanel, F. Louchet, and L. Truskinovsky, Phys. Rev. Lett. **114**, 105504 (2015).

[11] F. F. Csikor, C. Motz, D. Weygand, M. Zaiser, and S. Zapperi, Science **318**, 251 (2007).

[12] B. Jakobsen, H. F. Poulsen, U. Lienert, J. Almer, S. D. Shastri, H. O. Sorenson, C. Gundlach, and W. Pantleon, Science **312**, 889 (2006).

[13] A. J. Beaudoin, M. Obstalecki, W. Tayon, M. Hernquist, R. Mudrock, P. Kenesei, and U. Lienert, Acta Mater. **61**, 3456 (2013).

[14] J. C. Schuren, P. A. Shade, J. V. Bernier, S. F. Li, B. Blank, J. Lind, P. Kenesei, U. Lienert, R. M. Suter, T. J. Turner, D. M. Dimiduk, and J. Almer, Curr. Opin. Solid State Mater. Sci. **19**, 235 (2015).

[15] H. F. Poulsen, *Three-Dimensional X-Ray Diffraction Microscopy: Mapping Polycrystals and Their Dynamics*, Springer Tracts in Modern Physics (Springer, Berlin, 2004).

[16] H. F. Poulsen, S. F. Nielsen, E. M. Lauridsen, S. Schmidt, R. M. Suter, U. Lienert, L. Margulies, T. Lorentzen, and D. Juul Jensen, J. Appl. Crystallogr. **34**, 751 (2001).

[17] J. Oddershede, S. Schmidt, H. F. Poulsen, H. O. Sørensen, J. Wright, and W. Reimers, J. Appl. Crystallogr. **43**, 539 (2010).

[18] J. V. Bernier, N. R. Barton, U. Lienert, and M. P. Miller, J. Strain Anal. Eng. Des. **46**, 527 (2011).

[19] W. Tang, K. L. Halm, D. R. Trinkle, M. K. A. Koker, U. Lienert, P. Kenesei, and A. J. Beaudoin, Acta Mater. **101**, 71 (2015).

[20] A. L. Pilchak, Scr. Mater. **68**, 277 (2013).

[21] A. Fitzner, D. L. Prakash, J. Q. da Fonseca, M. Thomas, S.-Y. Zhang, J. P. Kelleher, P. Manuel, and M. Preuss, Acta Mater. **103**, 341 (2016).

[22] A. Venkataraman, P. A. Shade, R. Adebisi, S. Sathish, A. L. Pilchak, G. B. Viswanathan, M. C. Brandes, M. J. Mills, and M. D. Sangid, Metall. Mater. Trans. A **48**, 2222 (2017).

[23] T. J. Turner, P. A. Shade, J. V. Bernier, S. F. Li, J. C. Schuren, P. Kenesei, R. M. Suter, and J. Almer, Metall. Mater. Trans. A **48**, 627 (2016).

[24] P. A. Shade, D. B. Menasche, J. V. Bernier, P. Kenesei, J.-S. Park, R. M. Suter, J. C. Schuren, and T. J. Turner, J. Appl. Crystallogr. **49**, 700 (2016).

[25] B. A. Dowd, G. H. Campbell, R. B. Marr, V. V. Nagarkar, S. V. Tipnis, L. Axe, and D. P. Siddons, in *SPIE's International Symposium on Optical Science, Engineering, and Instrumentation* (SPIE, Bellingham, WA, 1999), pp. 224–236.

[26] Y. Wang, F. De Carlo, I. Foster, J. Insley, C. Kesselman, P. Lane, G. von Laszewski, D. C. Mancini, I. McNulty, M.-H. Su, and B. Tieman, in *SPIE's International Symposium on Optical Science, Engineering, and Instrumentation* (SPIE, Bellingham, WA, 1999), pp. 318–327.

[27] P. A. Shade, B. Blank, J. C. Schuren, T. J. Turner, P. Kenesei, K. Goetze, R. M. Suter, J. V. Bernier, S. F. Li, J. Lind, U. Lienert, and J. Almer, Rev. Sci. Instrum. **86**, 093902 (2015).

[28] J. V. Bernier, HEXRD, https://github.com/joelvbernier/hexrd.git

[29] While completeness is robust, it is biased towards larger grains when considering the intensity drop-off associated with the inclusion of higher-order and low-structure-factor reflections in the fitting. The χ^2 measure is less biased and will additionally filter out high completeness grains that are suspect, whether due to a high degree of overlapped signals, significant plastic deformation, or some other form of corruption.

[30] D. M. Dimiduk, E. M. Nadgorny, C. Woodward, M. D. Uchic, and P. A. Shade, Philos. Mag. **90**, 3621 (2010).

[31] J. Weiss and M. Carmen Miguel, Mater. Sci. Eng. A **387–389**, 292 (2004).

[32] N. Friedman, A. T. Jennings, G. Tsekenis, J.-Y. Kim, M. Tao, J. T. Uhl, J. R. Greer, and K. A. Dahmen, Phys. Rev. Lett. **109**, 095507 (2012).

[33] A. Clauset, C. R. Shalizi, and M. E. J. Newman, SIAM Rev. **51**, 661 (2009).

[34] J. Alstott, E. Bullmore, and D. Plenz, PLoS One **9**, e85777 (2014).

[35] See Supplemental Material at http://link.aps.org/supplemental/10.1103/PhysRevB.96.174116 for a video showing the difference result for resolved shear stress accompanies this paper. The symbols are located at the grain center of mass positions. The symbol color corresponds to the maximum resolved shear stress for basal slip systems in units of MPa. The size of the symbol is scaled to themagnitude of change in the effective stress for stress relaxation transients. This symbol size is interpolated linearly over three intermediate points between scans, to better illustrate the development of avalanches involving multiple grains. The symbol color is held constant over this interpolation of size. The video was prepared using ParaView, https://www.paraview.org/.

[36] D. C. Pagan, P. A. Shade, N. R. Barton, J.-S. Park, P. Kenesei, D. B. Menasche, and J. V. Bernier, Acta Mater. **128**, 406 (2017).

[37] H. Bauke, Eur. Phys. J. B **58**, 167 (2007).

[38] Q. H. Vuong, Econometrica **57**, 307 (1989).

[39] M. Zaiser and P. Moretti, J. Stat. Mech. (2005) P08004.

[40] M. Zaiser and N. Nikitas, J. Stat. Mech. (2007) P04013.

[41] P. A. Shade, R. Wheeler, Y. S. Choi, M. D. Uchic, D. M. Dimiduk, and H. L. Fraser, Acta Mater. **57**, 4580 (2009).

[42] M. Zaiser, B. Marmo, and P. Moretti, in *Proceedings of the International Conference on Statistical Mechanics of Plasticity and Related Instabilities* (SISSA, Trieste, 2005).

[43] M. J. Alava, L. Laurson, and S. Zapperi, Eur. Phys. J. Spec. Top. **223**, 2353 (2014).

[44] L. M. Brown, Mater. Sci. Technol. **28**, 1209 (2014).

[45] L. M. Brown, Philos. Mag. **96**, 2696 (2016).

[46] T. Neeraj and M. J. Mills, Mater. Sci. Eng. A **319–321**, 415 (2001).

[47] M. J. Blackburn and J. C. Williams, Trans. Am. Soc. Met. **62**, 398 (1969).

[48] J. C. Williams, R. G. Baggerly, and N. E. Paton, Metall. Mater. Trans. A **33**, 837 (2002).

[49] J. P. Sethna, M. K. Bierbaum, K. A. Dahmen, C. P. Goodrich, J. R. Greer, L. X. Hayden, J. P. Kent-Dobias, E. D. Lee,

D. B. Liarte, X. Ni, K. N. Quinn, A. Raju, D. Zeb Rocklin, A. Shekhawat, and S. Zapperi, Annu. Rev. Mater. Res. **47**, 217 (2017).

[50] V. Hasija, S. Ghosh, M. J. Mills, and D. S. Joseph, Acta Mater. **51**, 4533 (2003).

[51] A. S. Argon, Philos. Mag. **93**, 3795 (2013).

[52] H. Mughrabi, Metall. Mater. Trans. A **40**, 1257 (2009).

[53] Y. Cui, G. Po, and N. Ghoniem, Phys. Rev. Lett. **117**, 155502 (2016).